Valley-polarized magnetoconductivity and particle-hole symmetry breaking in a periodically modulated α-$\mathcal{T}_3$ lattice

SK Firoz Islam* and Paramita Dutta†
Institute of Physics, Sachivalaya Marg, Bhubaneswar 751005, India
(Received 15 December 2016; revised manuscript received 25 May 2017; published 17 July 2017)

We explore the transport properties of a periodically modulated α-$\mathcal{T}_3$ lattice in the presence of a perpendicular magnetic field. The effect of the Berry phase on electrical conductivity oscillation, so-called Weiss oscillation, caused by the modulation-induced nonzero drift velocity of charge carriers is investigated. Employing linear response theory within the low-temperature regime, we analyze Weiss oscillation as a function of the external magnetic field for both electrically and magnetically modulated α-$\mathcal{T}_3$ lattices numerically as well as analytically. The Berry phase makes this hexagonal lattice structure behave differently than other two-dimensional fermionic systems. It causes a significant valley polarization in magnetoconductivity. Most interestingly, the combined effect of both modulations breaks the particle-hole symmetry and causes a smooth transition from even (odd) to odd (even) filling fraction corresponding to the density of states peaks by means of the Berry phase.

DOI: 10.1103/PhysRevB.96.045418

I. INTRODUCTION

Since the discovery of the most celebrated atomically thin material, graphene [1,2], the search for new Dirac materials has been growing day by day owing to their peculiar electronic structure and possible applications for the next generation of nanoelectronics. The electronic properties of graphene, at low energy, are governed by the Dirac nature of its quasiparticle, which stems from its hexagonal lattice geometry [2]. A graphenelike two-dimensional (2D) lattice structure with an additional atom at the center of the hexagon can be realized in a $\mathcal{T}_3$ or dice lattice [3]. In contrast to graphene, the quasiparticles in this Dirac-Weyl material exhibit higher pseudospin $S = 1$ states [3]. Also, the presence of this additional atom at the center of the hexagon in the dice lattice gives rise to a dispersionless flat band at each Dirac point in addition to the Dirac cone found in graphene [3]. In recent times, this type of Dirac-Weyl material with higher spin states, $S = 1, 3/2, 2$, etc., is attracting much attention aimed at exploring the role of this additional atom in them [4]. A series of investigations has been carried out in order to reveal different aspects of the higher spin lattice [5–7].

A smooth transition from pseudospin $S = 1/2$ (graphene) to $S = 1$ (dice or $\mathcal{T}_3$ lattice) can be realized using the α-$\mathcal{T}_3$ model. Here, α is associated with the strength of the coupling of the central atom to its nearest neighbors. It has recently been demonstrated in $Hg_{1-x}Cd_xTe$ that, under a suitable doping concentration, this material can be mapped to the α-$\mathcal{T}_3$ model [4] with $\alpha = 1/\sqrt{3}$. Moreover, the continuous evolution of α from 0 (graphene) to 1 ($\mathcal{T}_3$) can be linked to a variable Berry phase by suitably parametrizing α [7]. The Berry phase, the geometrical phase arising during an adiabatic cyclic evolution of a quantum state, plays a vital role in explaining different properties of a system [8] such as the dc Hall conductivity [9], magnetotransport properties in the presence of randomly scattered charged impurities [10], and optical [4,11,12] properties. Note that the Berry phase is π and 0, respectively, in graphene and the $\mathcal{T}_3$ lattice, setting the two limits of the α-$\mathcal{T}_3$ system.

Magnetotransport measurements have always been appreciated for providing an efficient way to probe a 2D fermionic system. The presence of a magnetic field perpendicular to the plane of the system drastically changes the electronic band structure by the formation of discrete energy levels, i.e., Landau levels. Fluctuation of the chemical potential between different Landau levels with respect to the magnetic field manifests itself through the appearance of the well-known Shubnikov–de Hass oscillation in the longitudinal components ($\sigma_{xx/yy}$) of electrical conductivity [13]. On the other hand, off-diagonal components ($\sigma_{xy/yx}$) of the electrical conductivity tensor, i.e., quantum Hall conductivity, become quantized due to the incomplete cyclotron orbits of the electrons along the two opposite edges of the 2D system, transverse to the applied electric field [13].

In the presence of a perpendicular magnetic field, electrons do not posses any finite drift velocity inside the bulk of a 2D system. However, they may acquire a finite drift velocity if the system is subjected to an external perturbation. A magnetic-field-dependent oscillatory drift velocity can be imparted to electrons by applying an external perturbation which is periodic in space. This oscillatory drift velocity induces a new type of quantum oscillation in the magnetoresistance signal at a low range of magnetic field. This oscillation, known as Weiss oscillation, was first observed in magnetoresistance measurements in the electrically modulated usual 2D electronic systems [14–16]. Weiss oscillation, also known as commensurability oscillation, is caused by the commensurability of the two length scales, i.e., the radius of the cyclotron orbit near the Fermi energy and the period of the modulation [17–19]. Beenakker *et al.* [20] explained this oscillation using the concept of *guiding-center-drift resonance* between the periodic cyclotron orbit motion and the oscillating drift of the orbit center induced by the potential grating. From the application perspective, a modulated electric potential may result in a transition from semiconducting to semimetallic behavior of graphene [21]. Under an appropriate class of experimentally feasible one-dimensional external periodic potentials, electron beam supercollimation can be realized in graphene as suggested by Park *et al.* [22].

*firoz@iopb.res.in
†paramitad@iopb.res.in

Apart from the electric modulation scenario, magnetic modulation has also been considered theoretically [23–29], followed by several experiments [30–32]. In parallel, a wide range of applications has also been suggested by several groups. In 2007 Chieh *et al.* developed a magnetic-fluid optical-fiber modulator via magnetic modulation [33]. Even a usual 2D electron gas (2DEG) under a spatially modulated magnetic field can be used as a fantastic test bed to study resistivity induced by electron-electron scattering [34]. There are some other applications too [35].

Recently, the beating pattern in Weiss oscillation in Rashba spin-orbit coupled electrically/magnetically modulated 2DEG was investigated [36,37]. However, Matulis *et al.* have shown that Weiss oscillation can be enhanced in graphene due to the higher Fermi velocity associated with its linear massless energy dispersion [38]. Tahir *et al.* have studied the same but with magnetic modulation and predicted an enhancement of the amplitude and opposite phase in comparison to the case of electrically modulated graphene [39]. Similar investigations have been carried out in electrically modulated bilayer graphene [40] and silicene [41,42]. However, modulation-induced Weiss oscillation has not been addressed to date in the α-$\mathcal{T}_3$ system, to the best of our knowledge.

In this article, we investigate the behavior of Weiss oscillation aiming to explore the role of the variable Berry phase in it. Most interestingly, we find that the Berry phase causes a valley polarization in magnetoconductivity which is in contrast to that in graphene and usual 2DEG. Note that valley-polarized magnetoconductivity has been predicted in silicene too, but that is in the presence of spin-orbit interaction and a gate voltage [42]. However, when both types of modulations are considered together, the particle-hole symmetry of the system is broken, leading to an asymmetric density of states (DOS) in addition to the valley polarization in magnetoconductivity. We also notice a transition from odd (even) to even (odd) filling fraction corresponding to DOS peaks with the variation of the Berry phase.

Valley polarization in transport coefficients of the α-$\mathcal{T}_3$ lattice may have a possible application in valleytronics, a technology with control over the valley degree of freedom of the carriers [43–46]. Several proposals have been made for valleytronics devices that can be used in encoding or processing information [47] and, also, as valley filters or valley valves [48]. Intensive research on engineering potential valleytronic devices based on manipulating the valley nondegeneracy is needed in order to enrich this newly growing field more and more.

The remainder of this paper is organized as follows. In Sec. II, we describe our model Hamiltonian and the corresponding Landau levels. Our results on the effect of weak spatial modulation (both electric and magnetic cases separately) on energy levels, diffusive conductivity, and valley polarization are discussed in Sec. III. In Sec. IV we discuss the combined effects of electric and magnetic modulation. Finally, we summarize our results and conclude in Sec. VI.

II. MODEL HAMILTONIAN AND FORMATION OF LANDAU LEVELS

In Fig. 1 we present a schematic of an α-$\mathcal{T}_3$ lattice which consists of three atoms per unit cell, namely, A, B, and C.

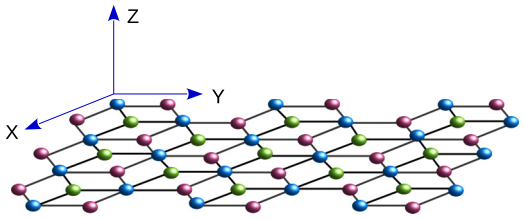

FIG. 1. Schematic of the α-$\mathcal{T}_3$ lattice. Colors denote three sublattices, i.e., A (magenta), B (blue), and C (green).

Atoms A and B form a honeycomb lattice structure similar to graphene with nearest-neighbor hopping amplitude t. The presence of an additional third atom, C, makes this lattice behave differently than graphene. In particular, atom C is connected to atom B with hopping amplitude αt ($\alpha < 1$).

Considering the three basis corresponding to the three atoms in the unit cell, the low-energy Hamiltonian of this system close to the Dirac points around a particular valley can be written as [7]

$$\mathcal{H}_0 = \begin{bmatrix} 0 & f_{\mathbf{p}}\cos\phi & 0 \\ f_{\mathbf{p}}^*\cos\phi & 0 & f_{\mathbf{p}}\sin\phi \\ 0 & f_{\mathbf{p}}^*\sin\phi & 0 \end{bmatrix}. \tag{1}$$

Here, $f_{\mathbf{p}} = v_F(\eta p_x - i p_y)$, where $\eta = \pm$ denotes the two valleys K and K', respectively, $\mathbf{p} = \{p_x, p_y\}$ is the 2D momentum vector, and v_F is the Fermi velocity. Note that the angle ϕ is parametrized by α via $\alpha = \tan\phi$ and the Hamiltonian is rescaled accordingly. The energy dispersion of the conic band can be readily obtained as $E_{k,\lambda} = \lambda\hbar v_F k$, where $\lambda = \pm$ correspond to the conduction and valence band, respectively. In addition to the conic bands there is a flat band with $E_{k,0} = 0\ \forall k$.

The full band structure of the α-$\mathcal{T}_3$ model is shown in Fig. 2. The eigenstates of the conic band are given by

$$\psi_\lambda = \begin{bmatrix} \cos\phi\ e^{i\theta_k} \\ \lambda \\ \sin\phi\ e^{-i\theta_k} \end{bmatrix}, \tag{2}$$

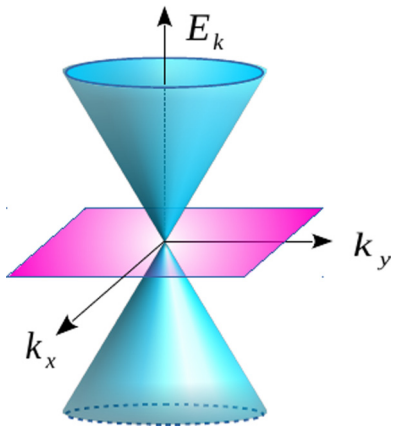

FIG. 2. Schematic of the band structure of an α-$\mathcal{T}_3$ lattice. The blue area represents the conic band structure, while the pink area denotes the dispersionless flat band.

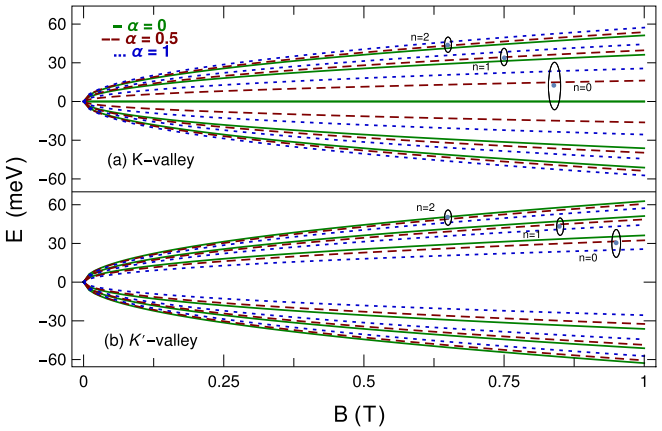

FIG. 3. Plot of a few Landau levels of the α-$\mathcal{T}_3$ lattice as a function of the magnetic field in the (a) K and (b) K' valleys for different values of α.

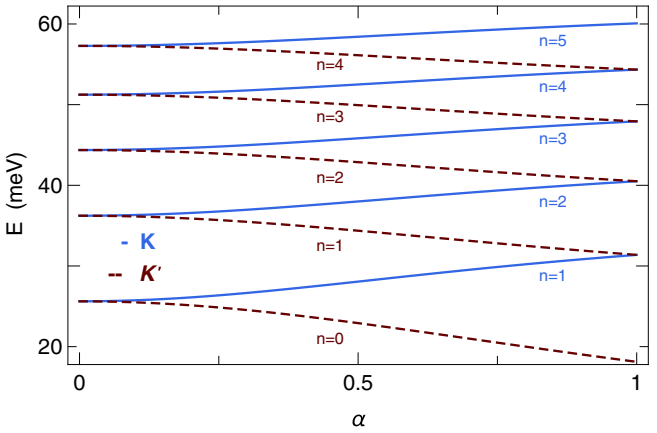

FIG. 4. Plot of the first few Landau levels of the α-$\mathcal{T}_3$ lattice as a function of α in the K and K' valleys at $B = 0.5$ T.

and for the flat band the same can be written as

$$\psi_0 = \begin{bmatrix} \sin\phi\, e^{i\theta_k} \\ 0 \\ -\cos\phi\, e^{-i\theta_k} \end{bmatrix}, \tag{3}$$

where $\theta_k = \tan^{-1}(k_y/k_x)$. The angle ϕ is connected to the Berry phase (Ω_η) in the conic band via $\Omega_\eta = \pi\eta\cos(2\phi) = \eta\pi(1-\alpha^2)/(1+\alpha^2)$. In contrast to graphene or the dice lattice the Berry phases in this lattice model corresponding to the two valleys are different from each other [7].

The application of a uniform magnetic field normal to the lattice plane (X-Y) can be incorporated via Peierls substitution $\Pi = (\mathbf{p} + e\mathbf{A})$, where the vector potential $\mathbf{A}$ is considered under Landau gauge as $\mathbf{A} = (-By,0,0)$ describing the magnetic field $\mathbf{B} = B\hat{z}$. Hence, the Hamiltonian near the Dirac point in the K valley reduces to

$$\mathcal{H}_K = \epsilon \begin{bmatrix} 0 & \hat{a}\cos\phi & 0 \\ \hat{a}^\dagger\cos\phi & 0 & \hat{a}\sin\phi \\ 0 & \hat{a}^\dagger\sin\phi & 0 \end{bmatrix}, \tag{4}$$

where $\epsilon = \hbar\omega_c$ with $\omega_c = \sqrt{2}v_F/l_c$. Here $l_c = \sqrt{\hbar/(eB)}$ is the magnetic length. Also, $\hat{a} = v_F\Pi_-/\epsilon$ and $\hat{a}^\dagger = v_F\Pi_+/\epsilon$ are the usual harmonic oscillator annihilation and creation operators, respectively, with $\Pi_\pm = \Pi_x \pm i\Pi_y$. The Hamiltonian for the K' valley can be obtained through the substitution $\hat{a} \to -\hat{a}^\dagger$. Hence, diagonalizing Eq. (4), one can directly obtain the Landau levels of the system in the form [7]

$$E_\xi^\lambda = \lambda\,\epsilon\sqrt{n+\chi_\eta}, \tag{5}$$

where $\xi \equiv \{n,\eta\}$ corresponds to a set of quantum numbers with $n = 0,1,2,\ldots$ being the Landau level index. The quantity χ_η is related to ϕ via the relation

$$\chi_\eta = [1 - \eta\cos(2\phi)]/2. \tag{6}$$

In Fig. 3, we show the nature of the first few Landau levels ($n = 0$, 1, and 2) as a function of the magnetic field for three values of α. There is a zero-energy Landau level for $n = 0$ in the K valley. On the other hand, the $n = 0$ level is of parabolic form in the K' valley. Note that, in graphene both valleys exhibit the $n = 0$ Landau level. The parabolic form can also be induced by tuning the Berry phase from zero to a finite value keeping the valley unaltered. The rest of the energy levels are shifted while the Berry phase is tuned. The Berry-phase-induced energy shift is positive for the K valley, while it is negative for the K' valley.

In Fig. 4, we show the variation of the first few Landau levels as a function of the Berry phase. It is evident from Fig. 4 that the nth Landau level of the K valley merges with the $(n+1)$th Landau level of the K' valley for $\alpha = 0$. The evolution of Landau levels was pointed out in Refs. [9,11].

The eigenfunction for $n > 0$ corresponding to the K valley is given by

$$\Psi_{n,k_x}^{\lambda,+}(\mathbf{r}) = \frac{e^{ik_x x}}{\sqrt{2L_x}} \begin{pmatrix} A^+\Phi_{n-1}\left[\frac{y-y_0}{l_c}\right] \\ \lambda\Phi_n\left[\frac{y-y_0}{l_c}\right] \\ B^+\Phi_{n+1}\left[\frac{y-y_0}{l_c}\right] \end{pmatrix}. \tag{7}$$

Here, the cyclotron orbit is centered at $y = y_0 = l_c^2 k_x$ and $\Phi_n(y) = [2^n n! l_c\sqrt{\pi}]^{-1/2}\exp(-y^2/2)H_n(y)$ is the usual harmonic oscillator wave function, where $H_n(y)$ is the Hermite polynomial of order n. The coefficients in Eq. (7) can be expressed as $A^\eta = \sqrt{n(1-\chi_\eta)/(n+\chi_\eta)}$ and $B^\eta = \sqrt{(n+1)\chi_\eta/(n+\chi_\eta)}$. For the zeroth Landau level, i.e., $n = 0$, the eigenfunction is given by

$$\Psi_{0,k_x}^{\lambda,+}(\mathbf{r}) = \frac{e^{ik_x x}}{\sqrt{2L_x}} \begin{pmatrix} 0 \\ \lambda\Phi_0\left[\frac{y-y_0}{l_c}\right] \\ \Phi_1\left[\frac{y-y_0}{l_c}\right] \end{pmatrix}. \tag{8}$$

The wave function in the K' valley can be obtained by performing the following transformations:

$$\Psi_{n,k_x}^{\lambda,-} = \Psi_{n,k_x}^{\lambda,+}[A^{+(-)} \to B^{-(+)}, \lambda \to -\lambda, \Phi_{n-1} \leftrightarrows \Phi_{n+1}]. \tag{9}$$

Note that, unlike monolayer graphene, the α-$\mathcal{T}_3$ lattice exhibits a dispersionless flat band too, which is well described in Ref. [10]. As we are considering a doped α-$\mathcal{T}_3$ lattice where the Fermi level is well inside the conic band, we ignore the effects of the flat band in our analysis.

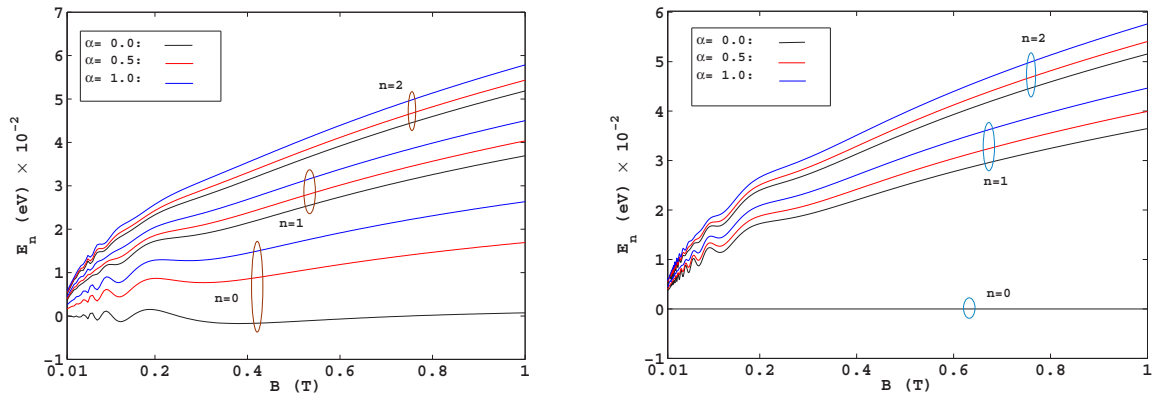

FIG. 5. First few modulated Landau levels in K valleys. (a) Electrically modulated and (b) magnetically modulated Landau levels. Here, the parameters are chosen to be modulation strength $V_e = V_m = 1$ meV, $k_x = 10^8$ m^{-1}, and modulation period $a = 350$ nm.

III. EFFECT OF ELECTRIC OR MAGNETIC MODULATION

A. Energy correction due to modulation

We assume in our analysis that the strength of the spatial electric/magnetic modulation is weak compared to the Landau level energy scale such that we can treat the modulation perturbatively. The first-order energy correction is evaluated in all cases by using the unperturbed eigenstates as follows.

1. Electric modulation

We describe our electrically modulated system by the Hamiltonian $\mathcal{H}_T^e = \mathcal{H}_\eta + V_e \cos(qy)$, where V_e is the strength of the electric modulation and $q = 2\pi/a$, where a is the period. Using perturbation theory, we evaluate the first-order energy correction for the K or K' valley as (for $n \geqslant 1$)

$$\Delta E^e_{\xi,k_x} = \int_0^{L_x} dx \int_{-\infty}^{\infty} \left[\Phi^{\lambda,\eta}_{n,k_x}(\mathbf{r})\right]^* V_e \cos(qy) \Phi^{\lambda,\eta}_{n,k_x}(\mathbf{r}) dy = \frac{V_e}{2} F_\xi(u) \cos(qy_0). \tag{10}$$

Here

$$F_\xi(u) = e^{-\frac{u}{2}}[|A^\eta|^2 L_{n-1}(u) + L_n(u) + |B^\eta|^2 L_{n+1}(u)], \tag{11}$$

where $L_n(u)$ is the Laguerre polynomial of order n and $u = q^2 l_c^2/2$. The total energy is now $E^e_{\xi,k_x} = E_\xi + \Delta E^e_{\xi,k_x}$, where k_x degeneracy is lifted. The energy correction to the ground state ($n = 0$) is

$$\Delta E^e_{\{0,+\},k_x} = \frac{V_e}{2} e^{-\frac{u}{2}}[L_0(u) + L_1(u)] \cos(qy_0). \tag{12}$$

In Fig. 5(a), the features of the first few modulated Landau levels of the K valley are shown as a function of the magnetic field for different values of α. For lower values of the magnetic field, electrical modulation induces a sinusoidal nature to the Landau level, and this feature slowly disappears with an increase in the Landau level index n. The qualitative behavior of the modulated energy levels in the K'-valley is similar to that in the K valley.

2. Magnetic modulation

Now we consider the case where the perpendicular magnetic field is weakly modulated without electric modulation. The dynamics of charge carriers under a modulated magnetic field is believed to be closely related to *composite fermions* in the fractional quantum Hall regime [49]. Under a weak magnetic field regime, theoretical works exist from the usual 2DEG to monolayer graphene (mentioned in Sec. I) exploring modulation-induced Weiss contribution. Along the same line, we investigate Weiss oscillation in a magnetically modulated α-$\mathcal{T}_3$ lattice.

First, we evaluate the first-order energy correction due to magnetic modulation. Let the perpendicular magnetic field be modulated very weakly as $\mathbf{B} = [B + B_m \cos(qy)]\hat{z}$, where $B_m \ll B$ describes the vector potential under the Landau gauge $\mathbf{A} = [-By - (B_m/q)\sin(qy), 0, 0]$. Similarly to the case of electric modulation, the total Hamiltonian can now be split into two parts as $\mathcal{H}_T^m = \mathcal{H}_\eta + \mathcal{H}_m$, where $\mathcal{H}_\eta$ is the unperturbed Hamiltonian and $\mathcal{H}_m$ is the modulation-induced perturbation, which can be written as

$$\mathcal{H}_m = \begin{bmatrix} 0 & \Upsilon\cos\phi & 0 \\ \Upsilon\cos\phi & 0 & \Upsilon\sin\phi \\ 0 & \Upsilon\sin\phi & 0 \end{bmatrix}, \tag{13}$$

where $\Upsilon = \eta e B_m v_F \sin(qy)/q$. Using the unperturbed wave function, the first-order energy correction due to magnetic modulation H_m can be evaluated as (for $n \geqslant 1$)

$$\Delta E^m_{\xi,k_x} = \frac{V_m}{2} G^\lambda_\xi(u) \cos(qy_0), \tag{14}$$

with $G^\lambda_\xi(u) = \lambda\eta R_{\{n,\eta\}}(u)$. For the K valley,

$$R_{\{n,+\}}(u) = \frac{2}{q l_c} e^{-\frac{u}{2}}[A^+ \Lambda_n(u)\cos\phi + B^+ \Lambda_{n+1}(u)\sin\phi], \tag{15}$$

with $\Lambda_n(u) = \sqrt{2n}\{L_{n-1}(u) - L_n(u)\}$ and $V_m = \hbar\omega_m$, where $\omega_m = e v_F B_m/q$. Similarly, one can obtain the first-order energy correction in the K' valley by interchanging the sine and cosine terms in $R_{\{n,-\}}(u)$, and $\lambda \to -\lambda$. Akin to the electric modulation case, here also we observe oscillation of the first few Landau levels due to the effect of magnetic modulation

for the same strength of modulation ($V_e = V_m = 1$ meV) as displayed in Fig. 5(b). Note that modulation does not have any effect on the first-order energy correction of the $n = 0$ level. This is shown by the straight horizontal line. In the K' valley, the behavior of the energy correction for different Landau levels is similar in nature qualitatively.

B. Diffusive conductivity

Under a low-temperature regime there are mainly two contributions to the longitudinal conductivity: one is the impurity-induced collisional conductivity and the other is the modulation-induced diffusive conductivity. However, the dominant contribution to the conductivity under a low magnetic field arises from the electron diffusion, caused by the applied in-plane weak spatial modulation. So, throughout the rest of the article, we use the term diffusive conductivity to refer to magnetoconductivity. On the other hand, the quantum Hall conductivity corresponding to the off-diagonal component of the conductivity tensor is neglected here due to the minor effect of the modulation as revealed in the literature [19]. In order to compute the diffusive contribution to the longitudinal conductivity, i.e., diffusive conductivity, we adopt the formalism developed in Ref. [50], which has been employed in the case of 2DEG [19] as well as graphene [38,39].

The dc diffusive conductivity can be evaluated by using the following semiclassical expression of the Kubo formula as [50]

$$\sigma_{\mu\nu} = \frac{\beta e^2}{\Omega} \sum_{\zeta} f_\zeta (1 - f_\zeta) \tau(E_\zeta) v_\mu v_\nu \tag{16}$$

provided the scattering processes involved are elastic or quasielastic. Here, $\zeta \equiv \{\xi, k_x\}$, and $f_\zeta = [1 + \exp\{\beta(E_\zeta - E_F)\}]^{-1}$ is the Fermi-Dirac distribution function, where E_F is the Fermi energy. In the above formula, $\tau(E_\zeta)$ denotes the energy-dependent collision time and $v_{\mu(\nu)} = (1/\hbar)\partial E_\zeta / \partial k_{\mu(\nu)}$, with $\mu(\nu) = x$ or y. $\Omega = L_x \times L_y$ is the dimension of the 2D lattice.

1. Electric modulation

We evaluate the drift velocity $v_{\mu(\nu)}$ in the presence of electric modulation. They are expressed as

$$v_x^e = \frac{1}{\hbar} \frac{\partial E^e_{\xi,k_x}}{\partial k_x} = -\frac{V_e}{\hbar q} u F_\xi(u) \sin(q y_0) \tag{17}$$

and $v_y^e = 0$. The latter suggests that diffusive conductivity arises along the direction normal to the applied modulation. Now we substitute v_x^e in Eq. (16) to obtain the diffusive conductivity. We replace the summation over k_x with the integral as $\sum_{k_x} \to \frac{L_x}{2\pi} \int_0^{L_y/l_c^2} dk_x$ using the fact that the origin of the cyclotron orbit is always confined within the system, i.e., $0 \leqslant |y_0| \leqslant L_y$. The factor $L_x/(2\pi)$ takes care of the periodic boundary condition. Thus the diffusive conductivity simplifies to

$$\sigma_{xx}^{e,\eta} = \frac{e^2}{h} \frac{\beta}{4\Gamma_0} V_e^2 u \sum_{\xi} f_\xi (1 - f_\xi) [F_\xi(u)]^2, \tag{18}$$

where Γ_0 is the impurity-induced broadening. Here, we assume that the collisional time $\tau(E_\xi)$ varies very slowly with the energy, i.e., $\tau(E_\xi) \simeq \tau_0$, which is a valid approximation under a low magnetic field, and also substitute $\Gamma_0 \approx \hbar/\tau_0$. The modulation effect on the Fermi distribution function is very small, and hence, we ignore it.

2. Magnetic modulation

Similarly to the case of electric modulation, the magnetic-modulation-induced drift velocity is given by

$$v_x^m = -\frac{V_m}{\hbar q} u G_\xi^\lambda(u) \sin(q y_0), \tag{19}$$

which leads to the exact form of the diffusive conductivity as

$$\sigma_{xx}^{m,\eta} = \frac{e^2}{h} \frac{\beta}{4\Gamma_0} V_m^2 u \sum_{\xi} f_\xi (1 - f_\xi) [R_\xi(u)]^2. \tag{20}$$

In comparison with the electric modulation scenario, the form of the drift velocity in the magnetic modulation case is exactly the same except for the term containing Laguerre polynomials [F_ξ(u) and $R_\xi(u)$ in the electric and magnetic modulation cases, respectively].

3. Discussion

To plot the diffusive conductivity for both the electric and the magnetic modulated systems we choose the following system parameters: modulation period $a = 350$ nm, temperature $T = 6$ K, strength of modulation $V_e = V_m = 1$ meV, and the impurity-induced Landau level broadening is assumed to be $\Gamma_0 = 1$ meV. We consider the Fermi energy which corresponds to the carrier density $n_e = 3 \times 10^{15}$ m^{-2}.

We show the behavior of the diffusive conductivity as a function of the magnetic field in Fig. 6 for both the electric [Fig. 6(a)] and the magnetic [Fig. 6(b)] modulation cases. We observe that under a low magnetic field ($B < 0.3$ T), the diffusive conductivity exhibits oscillation which is purely of the Weiss type. The variation of α as well as the Berry phase does not affect this type of oscillation significantly in this region. However, under the regime of a relatively higher magnetic field ($B > 0.3$ T), the effect of α becomes visible and it causes a phase shift to the Shubnikov–de Haas (SdH) oscillations, which are superimposed over the Weiss oscillation. Note that in the K valley the corresponding phase shift advances with an increase in α. On the other hand, it lags in the K' valley. The different Berry phases acquired by the electrons in the K and K' valleys are responsible for the difference in the phase modulation.

In order to understand the appearance of the valley-dependent phase shift in SdH oscillation over Weiss oscillation, we derive the approximate analytical form of the diffusive conductivity in each valley by replacing $\sum_n \to \pi l_c^2 \int D_\eta(E) dE$ in Eq. (18). Here, $D_\eta(E)$ is the density of states. Following the approach discussed in Ref. [51], we obtain the simplified form of the DOS as

$$D_\eta(E) = D_0 \left\{ 1 + 2\Omega(E) \cos\left[2\pi \left(\frac{E^2}{\epsilon^2} - \chi_\eta \right) \right] \right\}, \tag{21}$$

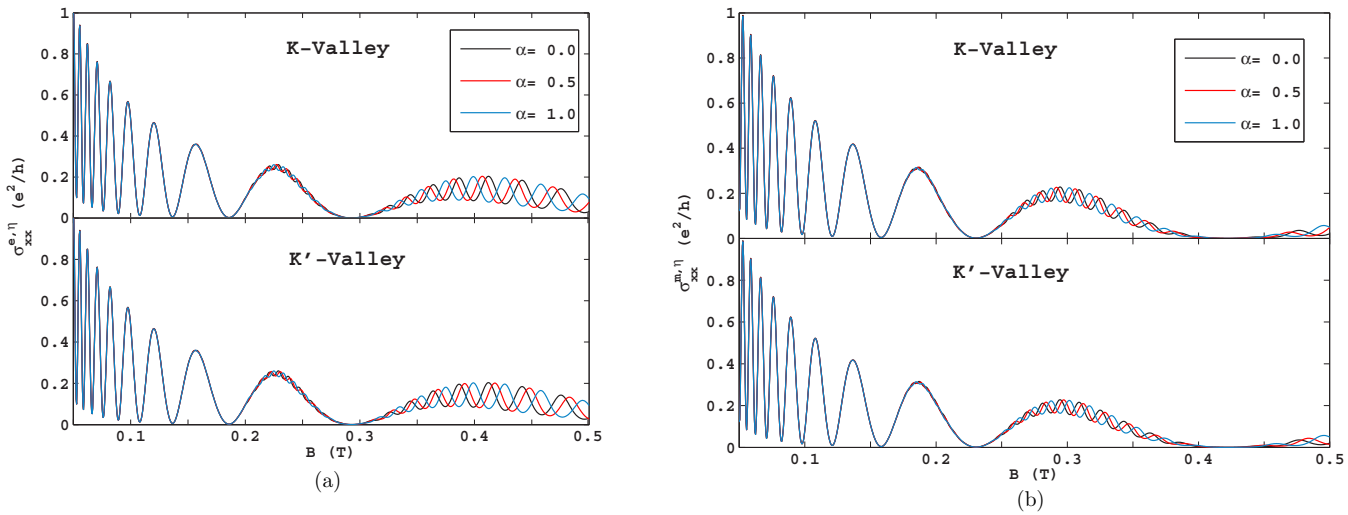

FIG. 6. Weiss oscillation for (a) electric modulation and (b) magnetic modulation. Variation of the diffusive conductivity is displayed as a function of the perpendicular magnetic field for the K (upper panels) and K' (lower panels) valleys using three values of the α.

where $D_0 = E/(2\pi\hbar^2 v_F^2)$ is the zero-magnetic-field DOS and impurity-induced damping factor

$$\Omega(E) = \exp\left\{-2\left(\frac{\pi E\Gamma(E)}{\epsilon^2}\right)\right\}, \tag{22}$$

with $\Gamma(E) \simeq 4\pi\Gamma_0^2 E/\epsilon^2$. After plugging it into Eq. (18) and using the higher Landau level approximation [19], i.e.,

$$e^{-u/2}L_n(u) \to \frac{1}{\sqrt{\pi}\sqrt{nu}}\cos\left(2\sqrt{nu} - \frac{\pi}{4}\right), \tag{23}$$

we have

$$\sigma_{xx}^{e,\eta} = \frac{e^2}{h}\frac{V_e^2}{\Gamma_0}\frac{\beta_W U_\eta}{32\pi^2}\left\{\mathcal{W}_e + 2\Omega(E_F)R^S\left(\frac{T}{T_S}\right) \times \cos\left[2\pi\left(\frac{g}{B} - \chi_\eta\right)\right]\cos^2\left[2\pi\left(\frac{f^\eta}{B} - \frac{1}{8}\right) - \theta_\eta^e\right]\right\}. \tag{24}$$

Here, $\beta_W = (k_B T_W)^{-1}$, with $T_W = ea v_F B/[4\pi^2 k_B(1 - \frac{\chi_\eta}{k_F^2 l_c^2})]$, is the characteristic temperature for Weiss oscillation and

$$U_\eta = [1 + (|A^\eta|^2 + |B_\eta|^2)\cos\nu + (|B^\eta|^2 - |A^\eta|^2)\sin\nu]^2 \tag{25}$$

at $n = n_F$ with $\nu = 2\pi/(ak_F)$. The appearance of a valley-dependent phase factor in the cosine square term is given by

$$\tan\theta_\eta^e = \frac{(|B^\eta|^2 - |A^\eta|^2)\sin\nu}{1 + (|A^\eta|^2 + |B_\eta|^2)\cos\nu}. \tag{26}$$

The first term in Eq. (24), $\mathcal{W}_e$, represents the pure Weiss oscillation, which is given by

$$\mathcal{W}_e = 1 - R^W\left(\frac{T}{T_W}\right) + 2R^W\left(\frac{T}{T_W}\right)\cos^2\left[2\pi\left(\frac{f^\eta}{B} - \frac{1}{8}\right) - \theta_\eta^e\right]. \tag{27}$$

The Weiss oscillation frequency $f^\eta = [1 - \chi_\eta(k_F^2 l_c^2)^{-1}]\hbar k_F/(ea)$, is weakly sensitive to the valley index and does not contribute sufficiently to the valley polarization. Also, it exhibits a valley-dependent phase factor (θ_η^e) which is too small to make any substantial changes between two valleys because of the small value of $\sin\nu$ in the numerator of Eq. (26).

The thermal damping factor describing the decay of the Weiss oscillation amplitude with increasing temperature is given by

$$R^W\left(\frac{T}{T_W}\right) = \frac{T/T_W}{\sinh(T/T_W)}. \tag{28}$$

Here, T_W determines the critical temperature beyond which Weiss oscillation starts to die out.

On the other hand, the second term in Eq. (24), containing the product of two cosines, represents the overlapping of SdH oscillation over Weiss oscillation with an increase in the magnetic field. The frequency of SdH oscillation ($g = \hbar k_F^2/e$) is independent of the valley index. The characteristic temperature for SdH oscillation is $T_S = (\hbar\omega_c)^2/(4\pi^2 E_F)$, with the thermal damping factor expressed as

$$R^S\left(\frac{T}{T_S}\right) = \frac{T/T_S}{\sinh(T/T_S)}. \tag{29}$$

Similarly to Weiss oscillation, T_S is the critical temperature for SdH oscillation. The critical temperature for Weiss oscillation under a particular magnetic field is higher than that for SdH oscillation.

From Eq. (24) it is observed that SdH oscillation superimposed over the Weiss region exhibits a valley-dependent phase factor, χ_η, which is the main reason behind the appearance of valley polarization in magnetoconductivity with increasing magnetic field. The presence of U_η in Eq. (24) indicates that the amplitudes of the oscillation in the two valleys are different for the entire range of the magnetic field, but its contribution to valley polarization is very small. The modulation-induced correction to the DOS [52] is of the order of $V_{e(m)}^2$ and

the corresponding correction to the diffusive conductivity becomes of the order of $V^4_{e(m)}$. This is very small and hence we neglect the modulation effect on the DOS.

For a particular valley, the Berry phase affects only the phase part, keeping the amplitude almost the same. This phase shift due to the Berry phase enters through the χ_η term, which is very clear in the higher-magnetic-field regime. In the context of amplitudes, U_η is not too sensitive to the Berry phase to be visualized.

Following the same procedure, we obtain the analytical expression of the diffusive conductivity for magnetic modulation as

$$\sigma_{xx}^{m,\eta} = \frac{e^2}{h}\frac{V_m^2}{\Gamma_0}\frac{\beta_W M_\eta}{32\pi^2}\left\{\mathcal{W}_m + 2\Omega(E_F)R^S\left(\frac{T}{T_S}\right) \times \cos\left[2\pi\left(\frac{g}{B}-\chi_\eta\right)\right] \times \sin^2\left[2\pi\left(\frac{f^\eta}{B}-\frac{1}{8}\right)-\theta_\eta^m\right]\right\}, \quad (30)$$

where $\mathcal{W}_m$ represents the pure Weiss oscillation, which is given by

$$\mathcal{W}_m = 1 - R^W\left(\frac{T}{T_W}\right) + 2R^W\left(\frac{T}{T_W}\right)\sin^2\left[2\pi\left(\frac{f^\eta}{B}-\frac{1}{8}\right)-\theta_\eta^m\right] \quad (31)$$

and

$$M_+ = \{[(A^+\cos\phi + B^+\sin\phi)(1-\cos\nu)]^2 + [(A^+\cos\phi - B^+\sin\phi)\sin\nu]^2\}^{1/2}. \quad (32)$$

The form of M_- can be obtained by just replacing $A^+ \to B^-$ and $B^+ \to A^-$. The phase factor is given by

$$\tan\theta_+^m = \frac{(A^+\cos\phi - B^+\sin\phi)\sin\nu}{(A^+\cos\phi + B^+\sin\phi)(1-\cos\nu)}. \quad (33)$$

The expression for the pure Weiss oscillation for magnetic modulation ($\mathcal{W}_m$) is similar qualitatively to that for electric modulation ($\mathcal{W}_e$) except they have opposite phases (provided θ_η^e and θ_η^m are very small) due to the presence of the squares of the sine and cosine functions in the two cases, respectively. This phase relationship is similar to that in the usual 2DEG and graphene, which was pointed out in Refs. [23,39].

From the above discussion it is clear that the diffusive conductivity is sensitive to the valley degree of freedom. Therefore, it is now of interest to examine the valley dependency of the diffusive conductivity in terms of the valley polarization with respect to the magnetic field as well as α.

C. Valley polarization

The valley polarization of diffusive conductivity can be defined as

$$P_v^\rho = \frac{\sigma_{xx}^{\rho,K} - \sigma_{xx}^{\rho,K'}}{\sigma_{xx}^{\rho,K} + \sigma_{xx}^{\rho,K'}}, \quad (34)$$

where ρ may be e or m, corresponding to the electric and magnetic modulation cases, respectively. We explore the valley polarization due to the finite differences in the diffusive conductivity in the two valleys at $\alpha = 0.5$. We calculate the valley polarization using Eq. (34) and depict the behavior of valley polarization with respect to the magnetic field in Figs. 7(a) and 7(b), which correspond to the electric and magnetic cases, respectively. We observe that under the low-magnetic-field regime where pure Weiss oscillation arises, the valley polarization is too small to be realized. However, with an enhancement of the magnetic field, when SdH oscillation starts to superimpose over Weiss, the polarization increases and rapidly oscillates. It is also possible to obtain 90% valley polarization under a high-magnetic-field regime. We show the result of valley polarization for a particular α. In order to examine the behavior of P_v as a function of the Berry phase we plot P_v vs α in the insets in Fig. 7. For this, we fix the magnetic field at the two values shown by the vertical arrows in Figs. 7(a) and 7(b), corresponding to the electric and

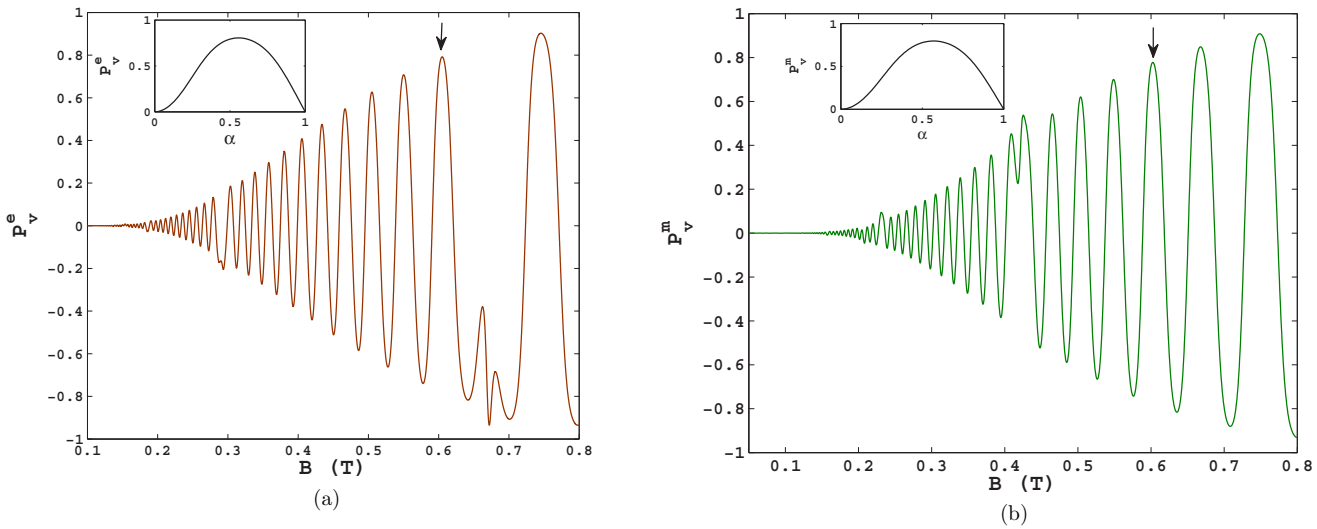

FIG. 7. Valley polarization (a) for electric modulation and (b) for magnetic modulation is plotted as a function of the magnetic field for $\alpha = 0.5$. Inset: Features of valley polarization with respect to α corresponding to the magnetic field indicated by the black arrow.

magnetic modulation cases, respectively. We note that valley polarization is maximum for the intermediate α, with zeros for the two limiting values of α (0 and 1) for both electric and magnetic modulations. For the two limiting values of α corresponding to graphene ($\alpha = 0$) and the dice lattice ($\alpha = 1$) the valley degeneracy is recovered and valley polarization disappears. Note that there are two dips in the P_e vs B profile, at around $B = 0.27$ and 0.65 T. Similarly, in the case of magnetic modulation the dips are around $B = 0.22$ and 0.42 T. All these dips correspond to the Weiss oscillation minima (see Fig. 6).

IV. COMBINED EFFECT OF ELECTRIC AND MAGNETIC MODULATION

So far, we have considered the role of electric and magnetic modulations in the transport phenomena separately. In this subsection, we examine what happens when both electric and magnetic modulation are considered simultaneously. The presence of magnetic stripes or a superconductor on the top of the system generally induces an unwanted electric potential modulation too, which motivated us to consider the effect of both modulations in the usual 2DEG also [23]. In our present case, the presence of both types of modulation induces first-order energy correction as

$$\Delta E^{\lambda}_{\xi,k_x} = \tfrac{1}{2}[V_e F_\xi(u) + \lambda\eta V_m R_\xi(u)]\cos(qy_0). \quad (35)$$

Note that unlike the previous cases, where either electric or magnetic modulation was considered, here the first-order energy correction breaks the particle-hole symmetry around zero energy, as $\Delta E^{+}_{\xi,k_x} \neq \Delta E^{-}_{\xi,k_x}$. This is one of the main results of our study. Note that this phenomenon could also be observed in Dirac material like graphene and silicene but this has not been pointed out in the literature, to the best of our knowledge. As stated before, the application of modulation manifests itself through a modulated density of states corresponding to the Landau level broadening. To gain more insight, in Fig. 8 we plot the modulated DOS as a function

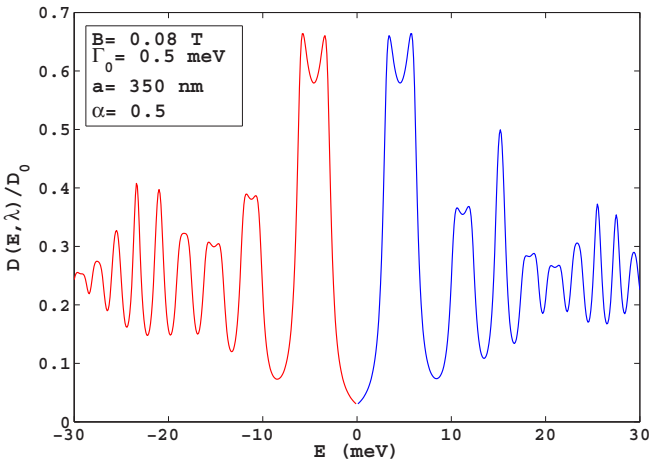

FIG. 8. Behavior of the modulated density of states in the presence of both types of modulations is shown for the K valley. The strengths of the electric and magnetic modulation are taken to be equal, i.e., $V_e = V_m = 1$ meV. The blue and red lines represent the conduction and valence band, respectively.

of the energy E in the presence of the combined effects of electric and magnetic modulation. The DOS in the presence of modulation can be expressed in a Lorentzian distribution as

$$\frac{D(E,\lambda)}{D_0} = \frac{(\hbar\omega_c)^2}{8\pi|E|}\sum_n \frac{1}{\pi}\int_0^{\pi} dc \frac{\Gamma_0}{\left(E - E^{\lambda}_{\xi,c}\right)^2 + \Gamma_0^2}, \quad (36)$$

with $D_0 = 2|E|/(\pi\hbar^2 v_F^2)$, $c = qy_0$, and $E^{\lambda}_{\xi,c} = \lambda\epsilon\sqrt{n+\chi_\eta} + V_0[F_\xi(u) + \lambda\eta R_\xi(u)]\cos(c)$, where $V_0 = V_e = V_m$. Interestingly, the electron and hole band lost the symmetry after the inclusion of both modulations here. The heights of particular peaks in the electron (conduction) and hole (valence) band are not the same. This is clearer in the higher-energy regime. We show the results for the K valley. Similar particle-hole symmetry breaking in the DOS can be obtained in the K' valley too.

The presence of both modulations together plays a vital role in transport phenomena of the usual 2DEG as observed in experiments [53] followed by theoretical work by Shi *et al.* [54], especially in the behavior of the DOS and conductivity with the filling fraction. The peculiar phenomenon of odd-even filling fraction transition in the DOS has been explored. Motivated by this, we investigated the phenomenon in our α-$\mathcal{T}_3$ model in order to reveal the role of the Berry phase in this context. In the left panel in Fig. 9 we show the behavior of the modulated DOS in the K valley with respect to the electron filling fraction, f_e, for the conduction band only. Here, (a), (b), and (c) represent the results for $\alpha = 0.1$, 0.5, and 1, respectively. We note that there is a transition of the peak positions from even to odd filling fraction when we tune α from 0 to 1 as depicted in the left panel in Fig. 9. We show the results for a higher filling fraction, which is inversely proportional to the magnetic field as $f_e = 2\pi n_e\hbar/eB$ for a fixed value of the carrier density. Now for 0 or very small value of α, the DOS shows some peaks at odd filling fraction, i.e., $f_e = 77, 79, 81$, and 83, and the rest are at even f_e. The DOS peaks at odd filling fraction indicate that the Landau levels are half-filled. On the contrary, when α is tuned to 1 (dice lattice), we observe exactly the inverted picture, i.e., all peaks (dips) positions get inverted to dips (peaks) as displayed in (c) (Fig. 9, left panel). These two patterns correspond to the two limiting values of α. There is a transition of the DOS peak positions from even to odd or from odd to even filling fraction through beating nodes for a particular value of α. In addition to this known feature, we note a similar odd (even)–even (odd) transition through a smooth variation of α from 0 to 1. At intermediate α, shown in (b) (Fig. 9, left panel), each odd (even) peak gets shifted from its earlier position for $\alpha = 0$, and they are neither at even nor at odd filling fraction; rather they arise at fractional values of f_e.

Now, we calculate the diffusive conductivity following an approach similar to that used in previous cases; it is given by

$$\sigma^{\lambda,\eta}_{xx} = \frac{e^2}{h}\frac{V_0^2\beta}{4\Gamma_0}u\sum_n f^{\lambda}_{\xi}\left(1 - f^{\lambda}_{\xi}\right)[F_\xi(u) + \lambda\eta R_\xi(u)]^2, \quad (37)$$

where λ is the band index. Both λ and η change their signs in the K' valley. Note that, unlike the previous cases of either electrically or magnetically modulated α-$\mathcal{T}_3$ lattices, here the diffusive conductivity depends on the band index too [see Eq. (37)]. This is because of the band-dependent group velocity, which arises from the first-order energy

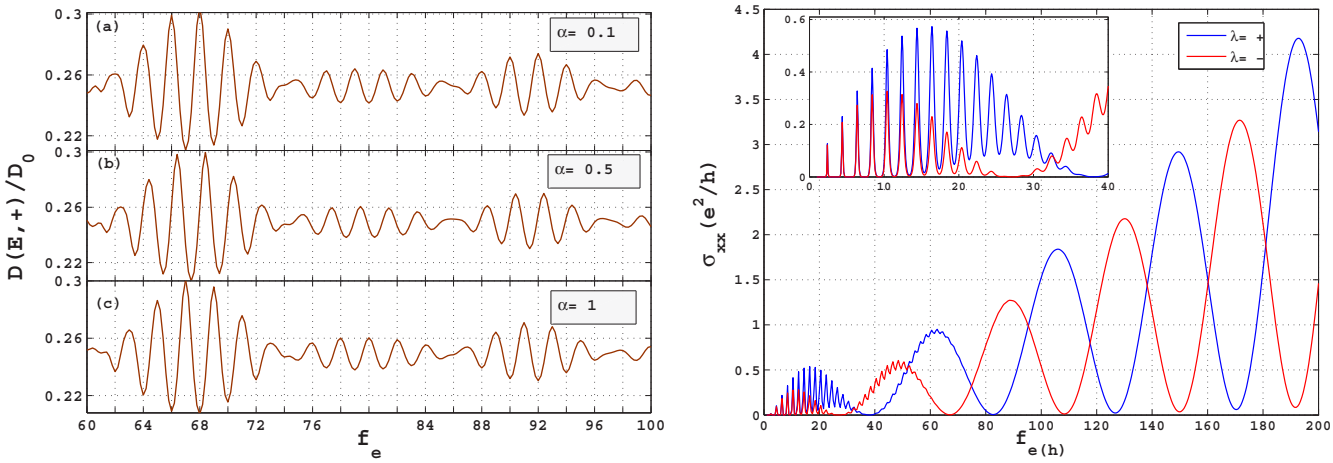

FIG. 9. Left: Modulated density of states in the K valley vs filling fraction f_e ($=2\pi n_e\hbar/eB$) for the conduction band is shown in the presence of both types of modulations for (a) $\alpha = 0.1$, (b) $\alpha = 0.5$, and (c) $\alpha = 1$. The carrier density is taken here as $n_e = 3 \times 10^{15}$ m^{-2} and the strength of modulation is taken to be $V_e = V_m = 1.2$ meV. Right: Variation of the diffusive conductivity with respect to the electron (hole) filling fraction $f_{e(h)}$ is plotted for the conduction (valence) band for the intermediate value of $\alpha = 0.5$ only.

correction due to the modulation of both types. A similar band dependence of the group velocity also appears in the case of magnetic modulation [Eq. (19)] but it does not affect the diffusive conductivity σ_{xx}'s being proportional to $(v_x^m)^2$ as expressed in Eq. (20).

We plot the diffusive conductivity for the K valley as a function of the filling fraction $f_{e(h)}$ for the conduction (valence) band, denoted by blue (red) curves in the right panel in Fig. 9. The amplitudes of the Weiss oscillations for both bands are enhanced due to the presence of both modulations. The diffusive conductivities for the conduction and valence bands are not similar to each other following the particle-hole asymmetry as shown in the DOS profile. There is a prominent phase difference between the Weiss oscillations for electron and hole bands. They change with the filling fraction as well as the magnetic field. This feature of Weiss oscillation is in complete contrast to the usual 2D gas because of the preservation of the particle-hole symmetry even in the presence of both modulations.

Finally, in Fig. 10 we present the variation of valley polarization in the diffusive conductivity as a function of the magnetic field using Eq. (34). In the presence of both modulations we observe that valley polarization naively remains unaltered from the case where we consider either electric or magnetic modulation. Here, we set $\alpha = 0.5$ considering the strengths of both modulations to be equal to each other i.e., $V_e = V_m = V_0$. However, from the realistic point of view their strengths may not be equal to each other. Also, the period of the modulations may be different. Note that, in Fig. 10 we consider two different periods for the two different types of the modulation. The valley polarization also does not change by an appreciable amount with their relative periods.

V. COMPARISON WITH OTHER 2D SYSTEMS

Now we draw a comparison between our present results and the existing results for other 2D systems like the usual 2DEG, graphene, and silicene. For the usual 2DEG, the first-order energy correction has been evaluated in Ref. [19] as

$$\Delta E^e_{k_x} = V_e^{2d} e^{-\frac{u}{2}} L_n(u)\cos(q y_0), \tag{38}$$

corresponding to the Landau levels $E_n = \hbar\omega_{2d}(n + 1/2)$ with $\omega_{2d} = eB/m^*$, m^* being the effective mass of the electrons in 2DEG. Using this correction the diffusive conductivity was evaluated in Ref. [19]. Note that, in the expression of the energy correction as well as in the diffusive conductivity for the α-$\mathcal{T}_3$ lattice we have summation over three successive Laguerre polynomials, whereas in 2DEG only one Laguerre polynomial is involved in the expression [see Eqs. (11) and (18)]. Moreover, in the α-$\mathcal{T}_3$ system both the energy correction and the diffusive conductivity are sensitive to the valley degree of freedom, whereas in a conventional 2DEG the issue of the valley degree of freedom is irrelevant.

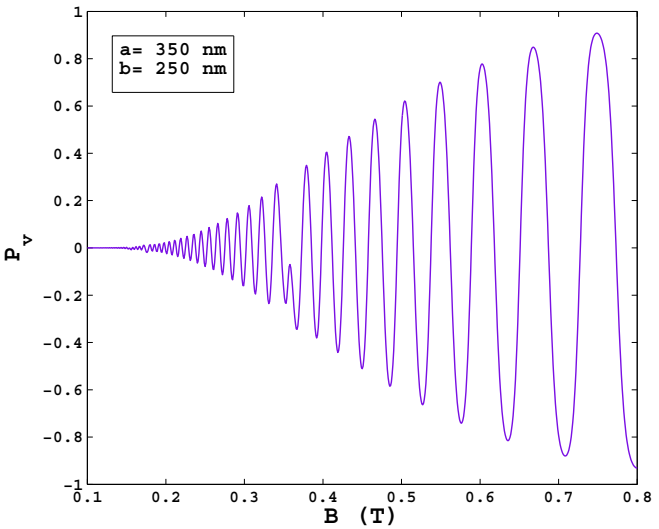

FIG. 10. Valley polarization in the presence of both modulations with $V_e = V_m = 1$ meV. The electric and magnetic modulation periods of are taken as a and b, respectively.

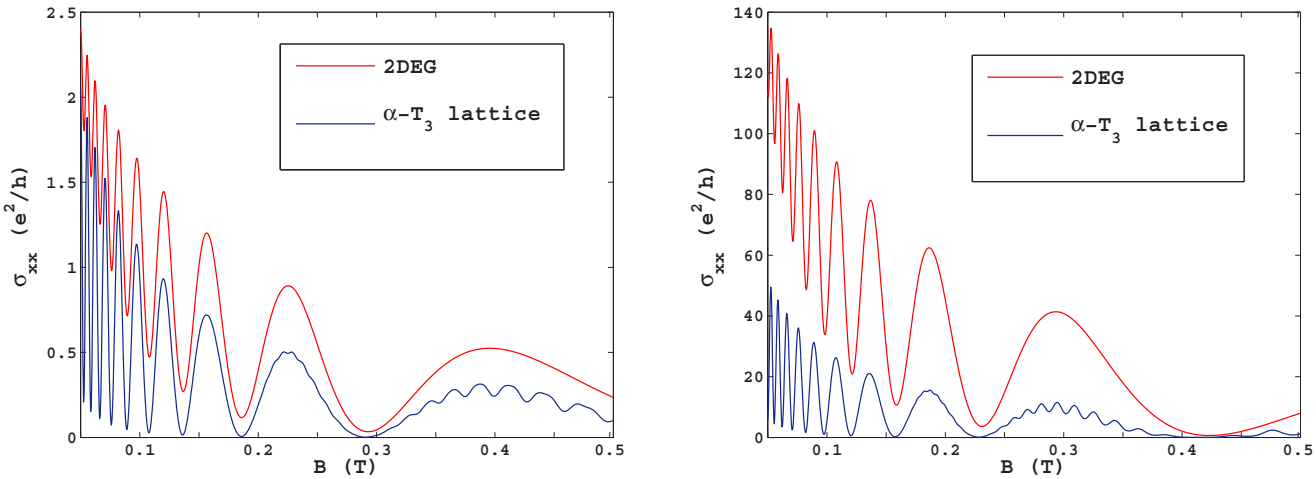

FIG. 11. Diffusive conductivity is plotted as a function of the magnetic field for the usual 2DEG and α-$\mathcal{T}_3$ lattice with $\alpha = 0.5$, taking contributions from both the valleys: (a) electric modulation and (b) magnetic modulation. In the case of magnetic modulation, the diffusive conductivity in the α-$\mathcal{T}_3$ lattice is multiplied by a factor of 25 in order to keep the scale the same as that for 2DEG.

Similarly, for magnetic modulation the first-order energy correction reads [23]

$$\Delta E^{m}_{k_x} = V^{2d}_{m} e^{-\frac{u}{2}} \left[\left(\frac{1}{2} - \frac{n}{u} \right) L_n(u) + \frac{n}{u} L_{n-1}(u) \right] \sin(q y_0) \tag{39}$$

and the corresponding diffusive conductivity can be found in Ref. [23]. Compared with Eqs. (15) and (20) it is clear that the summations over the Laguerre polynomial in both energy correction and diffusive conductivity corresponding to the two systems, α-$\mathcal{T}_3$ and usual 2DEG, are different from each other.

In Fig. 11 we plot both the electric [Fig. 11(a)] and the magnetic [Fig. 11(b)] modulation-induced diffusive conductivity for our system as well as 2DEG. For our numerical calculation the modulation strengths, electric as well as magnetic, in both systems are fixed to 1 meV. We find that the amplitude of Weiss oscillations in electrically modulated 2DEG is higher than that in the α-$\mathcal{T}_3$ model as depicted in Fig. 11(a). Also, they are naively in the same phase as each other. In the case of our system SdH oscillation starts to superimpose over Weiss oscillation under a relatively low-magnetic-field ($B \sim 0.3$ T) regime compared to that in 2DEG ($B > 0.5$ T). The reason is ascribed to the behavior of Landau levels with the magnetic field. In Dirac material the Landau level $E \propto \sqrt{B}$, whereas it is proportional to B in the usual 2DEG. Additionally, the presence of the Berry phase in the α-$\mathcal{T}_3$ model makes the diffusive conductivity behave differently in the two valleys leading towards the valley polarization. In the case of magnetic modulation, as displayed in Fig. 11(b), the order of magnitude of the diffusive conductivity is strongly suppressed in α-$\mathcal{T}_3$ in comparison to that in the usual 2DEG. This type of damped oscillation observed in the α-$\mathcal{T}_3$ lattice with respect to 2DEG is similar to that explored in graphene [39]. However, conductivity oscillations in the usual 2DEG and α-$\mathcal{T}_3$ are almost in phase. The most remarkable differences between these two systems are the appearance of valley polarization and particle-hole symmetry breaking in the α-$\mathcal{T}_3$ lattice in comparison to the usual 2DEG. The valley polarization in the α-$\mathcal{T}_3$ lattice is attributed to the valley-dependent mass term (χ_η) in Landau levels. The total energy correction due to the application of both modulations does not depend on the band index in the usual 2DEG, whereas it is strongly dependent on the band index (λ) in each valley of the α-$\mathcal{T}_3$ lattice [see Eq. (35)], leading towards the breaking of particle-hole symmetry.

Now we look into how the α-$\mathcal{T}_3$ system differs from graphene in diffusive conductivity. In our system, the first-order energy correction [see Eq. (10)] in the electric modulation case is weakly sensitive to the valley index and contains the summation of three successive Laguerre polynomials. On the other hand, there are summation over two successive Laguerre polynomials in case of graphene without any coefficient (see Ref. [38]). A similar difference in the form of the energy correction in both systems can also be observed in the magnetic modulation case. The results for $\alpha = 0$ correspond to graphene, as shown in Fig. 6, having features similar to those with the α-$\mathcal{T}_3$ lattice. However, the α-$\mathcal{T}_3$ lattice exhibits valley polarization in the diffusive conductivity with an increase in the magnetic field, which is absent in graphene due to the valley degeneracy in Landau levels. Similarly to the α-$\mathcal{T}_3$ lattice, the phenomenon of particle-hole symmetry breaking can also be obtained in graphene but it has not yet been pointed out in the literature, to the best of our knowledge.

A similar valley polarization has also been observed in electrically modulated silicene [42], even under a low-magnetic-field regime, but in the presence of a staggered potential between two sublattice planes. Weiss oscillation in magnetically modulated silicene has not been studied so far, to the best of our knowledge.

VI. SUMMARY AND CONCLUSION

To summarize, in this article we have theoretically studied magnetotransport properties of a spatially modulated α-$\mathcal{T}_3$ lattice. Both electric and magnetic modulation, individually as well as simultaneously, have been considered here. Using

the Kubo formula, based on linear response theory [55], we have obtained a modulation-induced additional contribution to the longitudinal conductivity, i.e., diffusive conductivity. The unique feature of the α-$\mathcal{T}_3$ lattice is the tunable Berry phase, which ranges from 0 to π. We have exploited this feature in order to reveal how it affects the quantum transport properties of the modulated α-$\mathcal{T}_3$ lattice. The presence of modulation imparts a nonzero drift velocity to the electrons which is oscillatory with the magnetic field and leads to the rise of Weiss oscillation in the electrical conductivity signal with the magnetic field. We have noted that a sizable valley polarization appears in the diffusive conductivity depending on the magnetic field. With the increase in the magnetic field, SdH oscillations start to superimpose over Weiss oscillations and valley polarization becomes much stronger and oscillates rapidly due to the strong dependence of the Landau levels on the Berry phase. To understand valley polarization with an increase in the magnetic field, we have derived an analytical form of the density of states and used it to get an approximate analytical expression for the diffusive conductivity. The signature of the Berry phase in the diffusive conductivity exclusively enters through the modification of Landau levels and the corresponding states of the system. On the contrary, we have also checked that in the absence of a magnetic field and modulation, the diffusive conductivity is independent of the Berry phase.

We have compared our results for the α-$\mathcal{T}_3$ lattice with the existing results in the literature for the usual 2DEG and other Dirac material such as graphene. We have observed that Weiss oscillation in the α-$\mathcal{T}_3$ lattice is almost in the same phase as the usual 2DEG except for an amplitude mismatch. The origin of the amplitude mismatch is due to the Dirac nature of band dispersion in the α-$\mathcal{T}_3$ lattice or graphene, which was pointed out in Ref. [38]. However, the most exciting physics of the α-$\mathcal{T}_3$ lattice is the appearance of valley polarization and particle-hole symmetry breaking in comparison to the usual 2DEG. On the other hand, though graphene and α-$\mathcal{T}_3$ lattice both exhibit a Dirac-like band dispersion, the presence of additional atoms at the center of each hexagon in the α-$\mathcal{T}_3$ lattice causes a valley polarization in diffusive conductivity which is absent in graphene. Moreover, graphene and α-$\mathcal{T}_3$ lattice both exhibit particle-hole symmetry breaking under the influence of both modulations. Very recently, the Carbotte group has shown that a small asymmetry in the energy band can be very sensitive to magneto-optical excitation [56,57]. Therefore, we conclude that the combination of both modulations can be used as a tool to break the particle-hole symmetry for manipulation of the valley degree of freedom in optical devices. Moreover, we have explored a modulation-induced transition of odd (even)-to-even (odd) filling fraction corresponding to DOS peaks with the variation of α.

As far as the practical realization of this α-$\mathcal{T}_3$ lattice is concerned, it can be naturally formed by growing a trilayer structure of cubic lattices in the (111) direction as shown by Wang *et al.* [58]. On the other hand, Bercioux *et al.* have proposed an experimental setup to realize this lattice by confining ultracold atoms to an optical lattice [59]. On the other hand, periodic modulation can be engineered in several ways. For example, Winkler *et al.* [14] have used an array of biased metallic strips on the surface of a 2D electronic system to achieve electric modulation. Magnetic modulation can be achieved by placing a few patterned ferromagnets or a superconductor on the surface of the 2D material [30–32].

ACKNOWLEDGMENTS

We especially acknowledge A. Saha for stimulating discussions and careful reading of the manuscript. S.F.I. also acknowledges T. K. Ghosh for useful discussions. P.D. thanks the Science and Engineering Research Board (SERB), Department of Science and Technology (DST), India, for financial support through a National Post-Doctoral Fellowship (File No. PDF/2016/001178). We acknowledge A. M. Jayannavar for his encouragement and support.

S.F.I. and P.D. contributed equally to this work.

[1] K. S. Novoselov, A. K. Geim, S. Morozov, D. Jiang, Y. Zhang, S. Dubonos, I. Grigorieva, and A. A. Firsov, Science **306**, 666 (2004).
[2] A. H. C. Neto, F. Guinea, N. M. R. Peres, K. S. Novoselov, and A. K. Geim, Rev. Mod. Phys. **81**, 109 (2009).
[3] J. Vidal, R. Mosseri, and B. Doucot, Phys. Rev. Lett. **81**, 5888 (1998).
[4] J. D. Malcolm and E. J. Nicol, Phys. Rev. B **92**, 035118 (2015).
[5] B. Dora, J. Kailasvuori, and R. Moessner, Phys. Rev. B **84**, 195422 (2011).
[6] Z. Lan, N. Goldman, A. Bermudez, W. Lu, and P. Ohberg, Phys. Rev. B **84**, 165115 (2011).
[7] A. Raoux, M. Morigi, J.-N. Fuchs, F. Piéchon, and G. Montambaux, Phys. Rev. Lett. **112**, 026402 (2014).
[8] D. Xiao, M. Chang, and Q. Niu, Rev. Mod. Phys. **82**, 1959 (2010).
[9] E. Illes, J. P. Carbotte, and E. J. Nicol, Phys. Rev. B **92**, 245410 (2015).
[10] T. Biswas and T. K. Ghosh, J. Phys.: Condens. Matter **28**, 366002 (2016).
[11] E. Illes and E. J. Nicol, Phys. Rev. B **94**, 125435 (2016).
[12] J. D. Malcolm and E. J. Nicol, Phys. Rev. B **93**, 165433 (2016).
[13] F. Duan and J. Guojin, *Introduction to Condensed Matter Physics*, Vol. 1 (World Scientific, Singapore, 2005); Y. Imry, *Introduction to Mesoscopic Physics* (Oxford University Press, New York, 1997).
[14] R. W. Winkler, J. P. Kotthaus, and K. Ploog, Phys. Rev. Lett. **62**, 1177 (1989).
[15] D. Weiss, K. von Klitzing, K. Ploog, and G. Weimann, Europhys. Lett. **8**, 179 (1989).
[16] R. R. Gerhardts, D. Weiss, and K. von Klitzing, Phys. Rev. Lett. **62**, 1173 (1989).
[17] P. Vasilopoulos and F. M. Peeters, Phys. Rev. Lett. **63**, 2120 (1989).
[18] C. Zhang and R. R. Gerhardts, Phys. Rev. B **41**, 12850 (1990).
[19] F. M. Peeters and P. Vasilopoulos, Phys. Rev. B **46**, 4667 (1992).

[20] C. W. J. Beenakker, Phys. Rev. Lett. **62**, 2020 (1989).
[21] J. H. Ho, Y. H. Chiu, S. J. Tsai, and M. F. Lin, Phys. Rev. B **79**, 115427 (2009).
[22] C.-H. Park, Y.-W. Son, L. Yang, M. L. Cohen, and S. G. Louie, Nano Lett. **8**, 2920 (2008).
[23] F. M. Peeters and P. Vasilopoulos, Phys. Rev. B **47**, 1466 (1993).
[24] P. Vasilopoulos and F. M. Peeters, Superlatt. Microstruct. **7**, 393 (1990).
[25] T. J. Li, S.-W. Gu, X. H. Wang, and J.-P. Peng, J. Phys.: Condens. Matter **8**, 313 (1996).
[26] A. Matulis and F. M. Peeters, Phys. Rev. B **62**, 91 (2000).
[27] A. S. Melnikov, S. V. Mironov, and S. V. Sharov, Phys. Rev. B **81**, 115308 (2010).
[28] D. P. Xue and G. Xiao, Phys. Rev. B **45**, 5986 (1992).
[29] G. Papp and F. M. Peeters, J. Phys.: Condens. Matter **16**, 8275 (2004).
[30] S. Izawa, S. Katsumoto, A. Endo, and Y. Iye, J. Phys. Soc. Jpn. **64**, 706 (1995).
[31] H. A. Carmona, A. K. Geim, A. Nogaret, P. C. Main, T. J. Foster, M. Henini, S. P. Beaumont, and M. G. Blamire, Phys. Rev. Lett. **74**, 3009 (1995).
[32] P. D. Ye, D. Weiss, R. R. Gerhardts, M. Seeger, K. von Klitzing, K. Eberl, and H. Nickel, Phys. Rev. Lett. **74**, 3013 (1995).
[33] J. J. Chieh, S. Y. Yang, H. E. Horng, C. Hong, and H. C. Yang, Appl. Phys. Lett. **90**, 133505 (2007).
[34] M. Kato, A. Endo, S. Katsumoto, and Y. Iye, Phys. Rev. B **58**, 4876 (1998).
[35] T. Mewes, C. K. A. Mewes, E. Nazaretski, J. Kim, K. C. Fong, Y. Obukhov, D. V. Pelekhov, P. E. Wigen, and P. C. Hammel, J. Appl. Phys. **102**, 033911 (2007).
[36] X. F. Wang, P. Vasilopoulos, and F. M. Peeters, Phys. Rev. B **71**, 125301 (2005).
[37] S. F. Islam and T. K. Ghosh, J. Phys.: Condens. Matter **24**, 185303 (2012).
[38] A. Matulis and F. M. Peeters, Phys. Rev. B **75**, 125429 (2007).
[39] M. Tahir and K. Sabeeh, Phys. Rev. B **77**, 195421 (2008).
[40] M. Zarenia, P. Vasilopoulos, and F. M. Peeters, Phys. Rev. B **85**, 245426 (2012).
[41] S. F. Islam and T. K. Ghosh, J. Phys.: Condens. Matter **26**, 335303 (2014).
[42] K. Shakouri, P. Vasilopoulos, V. Vargiamidis, and F. M. Peeters, Phys. Rev. B **90**, 125444 (2014).
[43] F. Qi and G. Jin, J. Appl. Phys. **115**, 173701 (2014).
[44] M. Ezawa, Phys. Rev. B **87**, 155415 (2013).
[45] O. Gunawan, Y. P. Shkolnikov, K. Vakili, T. Gokmen, E. P. De Poortere, and M. Shayegan, Phys. Rev. Lett. **97**, 186404 (2006).
[46] D. Xiao, W. Yao, and Q. Niu, Phys. Rev. Lett. **99**, 236809 (2007).
[47] J. R. Schaibley, H. Yu, G. Clark, P. Rivera, J. S. Ross, K. L. Seyler, W. Yao, and X. Xu, Nat. Rev. Mater. **1**, 16055 (2016).
[48] A. Rycerz, J. Tworzydło, and C. W. J. Beenakker, Nat. Phys. **3**, 172 (2007).
[49] A. Endo, M. Kawamura, S. Katsumoto, and Y. Iye, Phys. Rev. B **63**, 113310 (2001).
[50] M. Charbonneau, K. M. Van Vilet, and P. Vasilopoulos, J. Math. Phys. **23**, 318 (1982).
[51] SK F. Islam and T. K. Ghosh, J. Phys.: Condens. Matter **26**, 165303 (2014).
[52] SK F. Islam, N. K. Singh, and T. K. Ghosh, J. Phys.: Condens. Matter **23**, 445502 (2011).
[53] K. W. Edmonds, B. L. Gallagher, P. C. Main, N. Overend, R. Wirtz, A. Nogaret, M. Henini, C. H. Marrows, B. J. Hickey, and S. Thoms, Phys. Rev. B **64**, 041303 (2001).
[54] J. Shi, F. M. Peeters, K. W. Edmonds, and B. L. Gallagher, Phys. Rev. B **66**, 035328 (2002).
[55] P. Dutta, S. K. Maiti, and S. N. Karmakar, J. Appl. Phys. **112**, 044306 (2012).
[56] Z. Li and J. P. Carbotte, Phys. Rev. B **89**, 085413 (2014).
[57] C. J. Tabert and J. P. Carbotte, Phys. Rev. B **91**, 235405 (2015).
[58] F. Wang and Y. Ran, Phys. Rev. B **84**, 241103 (2011).
[59] D. Bercioux, D. F. Urban, H. Grabert, and W. Hausler, Phys. Rev. A **80**, 063603 (2009).